Mini-Seizures: Novel Interictal iEEG Biomarker Capturing Synchronization Network Dynamics at the Epileptogenic Zone

Authors: Tonmoy Monsoor [1], Sotaro Kanai [2], Atsuro Daida [2], Naoto Kuroda [3], Prateik Sinha [1], Shingo Oana [2], Yipeng Zhang [1], Lawrence Liu [1], Gaurav Singh [1], Chenda Duan [1], Myung Shin Sim [4], Aria Fallah [5], William Speier [6,7], Eishi Asano [3], Vwani Roychowdhury* [1], Hiroki Nariai* [2,8]

1. Department of Electrical and Computer Engineering, University of California, Los Angeles, Los Angeles, CA, USA
2. Division of Pediatric Neurology, Department of Pediatrics, UCLA Mattel Children's Hospital, David Geffen School of Medicine at UCLA, Los Angeles, CA, USA
3. Department of Pediatrics and Neurology, Children's Hospital of Michigan, Wayne State University School of Medicine, MI, USA
4. Department of Medicine, Statistics Core, University of California, Los Angeles, CA, USA
5. Department of Neurosurgery, David Geffen School of Medicine at UCLA, Los Angeles, CA, USA
6. Department of Radiological Sciences, University of California, Los Angeles, CA, USA
7. Department of Bioengineering, University of California, Los Angeles, CA, USA
8. The UCLA Children's Discovery and Innovation Institute, Los Angeles, CA, USA

***Corresponding Authors**

Hiroki Nariai, MD, PhD, MS (hnariai@mednet.ucla.edu) and Vwani Roychowdhury (vwani@g.ucla.edu)

Character count title:	115 characters (including space)
Word count abstract:	181 words
Word count text total:	5194 words (Introduction, Methods, Results, and Discussion)
Number of Tables:	1 for print, 0 for supplementary data
Number of Figures:	10 for print, 0 for supplementary data
Running Title:	Mini-seizures as a new EEG biomarker

DATA AVAILABILITY: Anonymized EEG data and metadata, including labels (channel's resection status, SOZ, patients' demographics, seizure outcomes, and pathology) used in this study are available on the OpenNEURO website (https://openneuro.org/datasets/ds005398).

ABSTRACT

Epilepsy affects 1% of the population, with up to one-third of patients being medication-resistant. Surgery is the only curative treatment, yet over one-third of surgical patients fail to achieve seizure freedom due to the lack of a reliable epileptogenic zone (EZ) biomarker. We introduced and validated mini-seizures, frequent hypersynchronization events at EZ hubs that mirror seizure network dynamics, as a novel interictal EEG biomarker. Using a dynamical networks-based model, we analyzed short interictal intracranial EEG from 159 patients across two institutions. Our model, integrating hypersynchronous network properties and clinical data, successfully identified EZ hubs and accurately predicted one-year postoperative seizure outcomes. Our model (mean F1 score: 87%) outperformed the high-frequency oscillations-based model (mean F1 score: 79%) and seizure onset zone resection-status-based model (current clinical standard) (mean F1 score: 78%), supporting its potential as a robust interictal biomarker for EZ localization. Our findings suggest mini-seizures and seizures exist on a continuum of epileptic events, sharing common network properties. Unlike seizure-based analyses that require 1-2 weeks of monitoring to capture spontaneous seizures, mini-seizures provide a rapid alternative using only brief interictal recordings.

INTRODUCTION

Epilepsy is one of the most common childhood neurological disorders, with an estimated prevalence of active epilepsy at 1%, affecting approximately 30 million children worldwide.[1, 2] Up to one-third of children with epilepsy are medication-resistant (defined by the failure of two tolerated and appropriately chosen antiseizure medications),[3] exhibiting significant risk of mortality and morbidity.[4] As many as 30-50% of children with drug-resistant epilepsy can be resective surgical candidates,[5] and epilepsy surgery is the only curative treatment for children with focal drug-resistant epilepsy and increases the likelihood of long-term survival[6] and improves the quality of life.[7] Achieving postoperative seizure freedom requires accurately identifying and removing or disrupting the epileptogenic zone (EZ)—the critical brain region responsible for generating seizures.[8] About 20-50% of them undergo invasive intracranial EEG (iEEG) monitoring, primarily when non-invasive evaluation fails to identify a clear focus.[9, 10] Typically, iEEG monitoring lasts 1–2 weeks to define the seizure onset zone (SOZ), defined as the brain region with channels displaying sustained rhythmic change on EEG clearly distinguished from state change and the baseline background activity, accompanied by habitual ictal behavioral change.[10, 11] However, this conventional approach using the SOZ to represent the EZ has significant limitations. Patients with infrequent seizures or multiple seizures may only exhibit a small number of target events during the limited time frame (hence, identified SOZ will be only a small part of the EZ),[10] and seizures may not occur at all during the hospitalization, leading to incomplete information on the SOZ.[12] At present, more than one-third of surgical patients do not achieve seizure freedom after surgery,[13] suggesting that the SOZ cannot fully capture the extent of the EZ. Moreover, the prolonged hospital stays required for iEEG monitoring are burdensome for children and their families. These challenges highlight the urgent need for tools leveraging short interictal (in-between seizure) EEG to identify the EZ, optimize postoperative seizure outcomes, and minimize the duration of long-term monitoring.

Emerging recognition is that focal epilepsy is a network disorder where critical nodes (the EZ hubs) involve peripheral nodes to synchronize epileptic networks.[14-16] Numerous studies on animal models and human research using neuroimaging and neurophysiology have demonstrated epilepsy involves network pathology.[17-19] Structural connectivity, evaluated using diffusion MRI,[20], and functional connectivity, evaluated through magnetoencephalography,[21] functional MRI (fMRI),[22, 23] and intracranial EEG (iEEG),[19, 20] have revealed abnormal connectivity patterns in patients with epilepsy. Currently, the clinical practice relies primarily on seizures, which account for less than 1% of collected iEEG data, and is agnostic to the remaining 99% of interictal iEEG data.

Our overarching hypothesis is that the synchronized epileptic network events –resulting from the underlying pathophysiology of epilepsy– form a continuum: Smaller, more frequent hyper-

synchronization events (mini-seizures) occur spontaneously during interictal periods and engage the same EZ hubs and synchronization pathways that drive less frequent, larger events (seizures). This hypothesis is grounded on a shared behavior exhibited by most bursty complex dynamical systems, where a stream of smaller events of varying magnitudes occur continually, and as an integral part of the same continuum of events, rare large events occur that are felt throughout the system.[24-31] In the current study, we propose the High-Frequency Synchronization Network Dynamics (HiSyncDx) platform, a novel data-driven framework designed to capture dynamic and complex synchronization patterns and identify hubs within epileptic networks (EZ hubs) by leveraging graph theory and parallel computing applied on iEEG data to estimate interactions across thousands of potential channel pairs with hundreds of milliseconds resolution. We analyzed a large cohort of patients with focal drug-resistant pediatric-onset epilepsy who underwent iEEG monitoring to test our hypothesis.

METHODS:

Study Cohort:

This was a multi-institutional retrospective cohort study. The inclusion criteria consisted of [a] having pediatric-onset (up to age 21 years) focal drug-resistance epilepsy, [b] simultaneous video-iEEG recording with subdural grid/strip for epilepsy surgery between August 2016 and December 2023 at UCLA Mattel Children's Hospital (UCLA) or between January 2007 and May 2018 at Children's Hospital of Michigan, Detroit (Detroit), [c] iEEG sampling rate of at least 1,000Hz, [d] iEEG contained at least an artifact-free 20 min slow-wave sleep epoch at least two hours apart from clinical seizure events, [e] undergoing resection surgery after iEEG recording, and [f] known postoperative seizure outcomes over one year. The exclusion criteria included [a] undergoing epilepsy surgery without iEEG recording (such as hemispherectomy or neuroimaging-guided resection), [b] the presence of massive brain malformations (such as megalencephaly and perisylvian polymicrogyria) or previous surgeries that make it difficult to identify brain anatomy during the iEEG study, and [c] patients without one-year postoperative seizure outcomes. The institutional review board at UCLA and Wayne State University have approved the protocol. We obtained written informed consent from patients or the guardians of pediatric patients.

Patient evaluation:

All study subjects were referred during the study period underwent a standardized presurgical evaluation, which—at a minimum—consisted of inpatient video-EEG monitoring, high resolution (3.0 T) brain magnetic resonance imaging (MRI), and 18 fluoro-deoxyglucose positron emission tomography

(FDG-PET), with MRI-PET co-registration.[32, 33] The margins and extent of resections were determined mainly based on the SOZ, clinically defined as regions initially exhibiting sustained rhythmic waveforms at the onset of habitual seizures. In some cases, the seizure onset zones were incompletely resected to prevent an unacceptable neurological deficit. Postoperative seizure outcomes were determined based on the status of ILAE class I outcomes (seizure-free) versus others 12 months after the resective surgery.

iEEG recording:

Macroelectrodes, including platinum grid/strip electrodes (10 mm intercontact distance), were surgically implanted. The placement of intracranial electrodes was guided by the results of scalp video-EEG recording and neuroimaging studies.[32, 33] All electrode plates were stitched to adjacent plates, the edge of the dura mater, or both to minimize movement of subdural electrodes after placement. Both institutions obtained iEEG recordings using Nihon Kohden Systems (Irvine, California, USA). The sampling frequency was set at 1,000 Hz in Detroit and at 2,000 Hz in UCLA upon acquisition.

Acquisition of three-dimensional (3D) brain surface images:

We obtained preoperative high-resolution 3D magnetization-prepared rapid acquisition with gradient echo (MPRAGE) T1-weighted image of the entire head. Using the FreeSurfer scripts,[34] we created the averaged surface image for which all electrode locations were spatially normalized.[32, 33] In cases where the software failed to detect the pial surface accurately due to insufficient cerebral myelination, we manually delineated the pial surface using the Control Point function. The averaged surface image functioned as the template for the analysis of anatomical location.

Electrode co-registration of brain MRI and standardized parcellation of regions of interest (ROIs):

For the dataset from UCLA, each implanted contact was labeled visually according to the Desikan-Killiany-Tourville atlas.[35] The location of electrodes was directly defined within a Freesurfer-based 3D surface image using post-implant computed tomography (CT) images using Brainstorm software.[36] For the dataset from Detroit, all implanted subdural contacts were coregistered with 3D surface images within the FreeSurfer with an FSaverage vertex label.[32] For the data harmonization between the two institutions, the FSaverage vertex of Detroit datasets was converted to MNI coordinates.[37] Finally, these data were combined with UCLA patients, which were projected to the MNI normalized space under Brainstorm for the co-registration image. After the co-registration procedure, iEEG electrode contacts outside of the brain or with significant artifacts were excluded for subsequent EEG analysis. The

channel resection status (resected vs. preserved) was meticulously determined based on post-resection brain MRI and intraoperative pictures (pre-and post-resection) to visually confirm the grid/strip locations).[32, 33, 38]

iEEG data pre-processing:

The EEG data from UCLA was first resampled to be the same sampling frequency of 1,000 Hz to match that from Wayne State, and a band-reject filter was to reject the 60 Hz and its harmonics with a stopband of 2 Hz. The signals were referenced using a bipolar montage. Five-minute long interictal iEEG data from each patient will be obtained on the first night of the monitoring, before the medication wean.

Building high-frequency synchronization network HiSyncDx:

For a given frequency band, we construct a directed weighted time-varying synchronization network from the iEEG using the following steps (see **Figure 1**):[39]

- Split the iEEG data into T-second-long non-overlapping data segments. For each data segment, we construct a directed weighted network following the steps below.
- The network consists of N nodes where N is the number of channels in iEEG
- The edge weights between the nodes in the network are computed using the power and phase-related coupling coefficient, which are computed from the Fourier transform
- The directionality between the edges is computed using the phase-related coupling coefficient
- A dynamic threshold is used to only keep edge weights in the top 90% percentile

Power and Phase spectrum using Fourier transform: For each channel, we compute its power and phase spectrum using Fast Fourier Transform (FFT). After obtaining its power spectrum, we isolate the given frequency band and set the magnitude of each frequency component outside the given band to zero.

Power-related coupling coefficient between node i and j: Let P_i be the sum of the squared power spectrum of the ith node and is given by

$$\mathcal{P}_i = \sum_{k=1}^{K} |P_{i,k}|^2$$

where K is the number of discrete frequencies in the given frequency band. Then, power-related coupling coefficient between nodes i and j is given by

$$\sigma_{ij}^{\mathcal{P}} = \mathcal{P}_i + \mathcal{P}_j$$

Phase-related coupling coefficient between node i and j: Phase-related coupling coefficient between node i and j is given by

$$\sigma_{ij}^{\phi} = -\sigma_{ji}^{\phi} = \frac{1}{K}\sum_{k=1}^{K}\sin(\phi_{j,k} - \phi_{i,k})$$

where K is the number of discrete frequencies in the given frequency band.

Edge weight between node i and j: The synchronous coefficient between node i and j, d_{ij} is given by

$$d_{ij} = \sigma_{ij}^{\mathcal{P}}\sigma_{ij}^{\phi}$$

From the above equation, it can be observed that the synchronous coefficient is the product of the power and phase-related coefficient. Then, we compute the edge weight between node i and j, w_{ij}, as

$$w_{ij} = 1 - exp(-||d_{ij}||^{\gamma})$$

where we use the exponentiation factor

$$\gamma = 1$$

Directionality to the edge between node i and j: The total phase in node j is given by

$$\eta_j^{\phi} = \sum_{k=1}^{K}\phi_{j,k}$$

where K is the number of discrete frequencies in the given frequency band. Analogously, the total phase in node i is given by

$$\eta_i^{\phi} = \sum_{k=1}^{K}\phi_{i,k}$$

where K is the number of discrete frequencies in the given frequency band. If there is a greater total phase in node j than node i, that is

$$\eta_j^{\phi} > \eta_i^{\phi}$$

then the weighted edge points from node i to node j (i $\Rightarrow$ j). If there is a greater total phase in node i than node j, that is

$$\eta_i^{\phi} > \eta_j^{\phi}$$

then the weighted edge points from node j to node i (j $\Rightarrow$ i).

Computing Network Synchronization Index, Node Properties, and Other Characteristics of High-Frequency Synchronization Networks

For each of the three frequency bands, HiSyncDx outputs a sequence of T networks (assuming one-second-long segments) where T is the duration of the iEEG recordings. To explore the structure and the dynamics of the networks, we use a mix of global (network level) and local (node level) graph-theoretic properties. We hypothesize that mini-seizures are driven by the EZ region (represented by a few nodes in the network), leading to large-scale/intensity network synchronization events, such as seizures. To capture such events in the network level dynamics, we use measures such as (i) Fiedler eigenvalue: higher Fiedler eigenvalue implies higher synchronizability of the networks, (ii) edge weights: larger edge weight implies stronger synchronization strength and (ii) Node degree variance: higher variance implies the presence of hubs. We propose a data-driven computational metric to quantitatively identify synchronization networks that have high values for each of the metrics. We refer to this metric as the Network Synchronization Index (SI), which is the product of the three global measures stated above. The metric not only assists in identifying the events but also provides a potential framework for ranking the network states and unearthing interictal time stamps of interest in an unsupervised way. In addition to identifying such events, we also identify the drivers of such events using a set of node-level features like in-degree,out-degree, scaled in and out degrees by Fiedler eigenvalue and eigencentrality scores.

HiSyncDx-based EZ prediction: defining EZ centrality score

As mentioned in the previous section, we aim to identify the drivers of the network synchronization events (EZ hubs) (**Figure 2**). To quantify the importance of each electrode channel (EZ centrality score), a set of five network features—including in-degree, out-degree, eigenvector centrality, and Fiedler eigenvalue-based measures—are extracted at each time point. These features are summarized

across time by measuring their mean, variance, skewness, and kurtosis, forming a 20-dimensional feature vector for each channel in each frequency band. For each channel, the 20-dimensional feature vectors for each of the three frequency bands is concatenated into a single 60-dimensional feature matrix. The resulting feature matrix is then used as input for a random forest classifier, trained using a 10-fold cross-validation strategy, with the SOZ (seizure onset zone) information serving as binary ground truth labels. The random forest classifier outputs an EZ centrality score that can be thresholded to identify the EZ. This method provides an interpretable, data-driven approach to localizing the EZ, leveraging high-frequency synchronization dynamics to improve diagnostic precision.

Predicting surgical outcomes using EZ centrality scores

To evaluate the EZ centrality scores as interictal iEEG markers of the EZ, we tested their efficacy in predicting surgical outcomes (**Figure 3**). We construct a 3-dimensional feature vector from the EZ centrality scores: catEZ, resEZ, and resection, where:

$$\mathbf{catEZ} = \begin{cases} 1 & \text{if all channels predicted to be EZ are resected,} \\ 0 & \text{otherwise,} \end{cases}$$

$$\mathbf{resEZ} = \frac{\sum_{i \in \mathbf{resEZ}} P(i \in \mathbf{EZ})}{\sum_{i \in \mathbf{all}} P(i \in \mathbf{EZ})},$$

$$\mathbf{resection} = \frac{\sum_{i \in \mathbf{resEZ}} P(i \in \mathbf{EZ}) + \sum_{i \in \mathbf{resnonEZ}} P(i \in \mathbf{EZ})}{\sum_{i \in \mathbf{all}} P(i \in \mathbf{EZ})}.$$

We augmented the EZ centrality scores with patient demographics (age and sex) to obtain a five-dimensional feature vector for surgical outcome prediction. We trained and validated the performance of the five-dimensional surgical outcome prediction model on the same multicenter patient corpus of 159 patients that we introduced earlier. Since the patient cohort is unbalanced, with ~70% of patients being seizure-free and ~30% of patients being non-seizure-free, we used 10-fold stratified cross-validation to evaluate our model's performance and generalization power. In 10-fold stratified cross-validation, we split the corpus of 159 patients into 10 patient groups of roughly equal size, where each group has around 70% seizure-free and around 30% non-seizure-free patients. Then, for each fold, we train the model using nine patient groups and then test the model on the left-out patient group.

Statistical analysis

Statistical analyses were performed using Python (3.9.1). Quantitative data were reported as medians with interquartile ranges or means with standard deviations. Group comparisons used chi-square tests for distributions and Student's t-tests for means, with significance set at $p < 0.05$ unless stated

otherwise. Machine learning model performance was evaluated using accuracy and F1 score. Specific statistical tests for each experiment are detailed in their respective sections.

RESULTS:

Cohort characteristics

We studied 159 patients (79 females) from two centers who met the eligibility criteria (**Table 1**). The median age at surgery was 12 years (range: 3–44 years). The median duration of analyzed EEG data was 91.5 minutes [IQR: 90.6–96.6 min] for the UCLA dataset and 5.3 minutes [IQR: 5.1–5.7 min] for the Detroit dataset. All patients underwent resective surgery, with 110 patients (69.2%) achieving seizure freedom. The pathological diagnoses included focal cortical dysplasia (FCD) (40.3%), tumor (19.5%), hippocampal sclerosis (HS) (6.9%), and other conditions (33.3%).

Novel interictal biomarker: high-frequency synchronization network dynamics and mini-seizures

Interictal hypersynchronous network states mimic Ictal network states.

Analysis of HiSyncDx networks revealed distinct patterns of hypersynchrony across both interictal and ictal periods of EEG recordings (**Figure 4**). During interictal periods, we observed transient hypersynchronous states that manifested as "mini-seizures," characterized by brief periods of increased network connectivity. These interictal networks showed a consistent pattern of organization centered around the seizure onset zone (SOZ). Notably, the network topology during these interictal events showed remarkable similarity to ictal patterns, suggesting a common underlying pathophysiological mechanism. In the ictal segments, the EEG recordings captured the evolution of full seizure activity, marked by the emergence of pronounced hypersynchronous states at seizure onset. The network representations reveal a more extensive recruitment of brain regions during the ictal period, with the SOZ maintaining its central role in the network architecture. This analysis demonstrates HiSyncDx's capability to identify and characterize hypersynchronous states across different temporal scales, providing insight into the relationship between interictal network dynamics and seizure generation.

Mini-seizures have salient features in the synchronization index space.

Our analysis established a quantitative framework for distinguishing mini-seizures from normal brain states through network characteristics and synchronization metrics (Figure 5). The network topology during normal states exhibited markedly different properties compared to mini-seizure states. In normal network states, we observed low synchronizability as measured by the Fiedler eigenvalue, minimal

synchronization strength indicated by low average giant connected component edge weights, and an absence of synchronization hubs evidenced by low degree variance across nodes. In contrast, mini-seizure states demonstrated significantly enhanced network synchronization properties, characterized by high Fiedler eigenvalues, increased edge weights in the giant connected component, and the emergence of distinct synchronization hubs with high degree variance. The synchronization index distribution revealed a clear bimodal pattern, enabling the definition of distinct regimes: a normal regime (synchronization index < 3) and a mini-seizure regime (synchronization index ≥ 3). Notably, the analysis revealed a hierarchical organization of synchronization states, where interictal mini-seizures (shown in blue) exhibited intermediate synchronization indices between normal states and full ictal seizures (shown in red). This quantitative characterization provided an objective, data-driven approach for detecting and classifying mini-seizures in interictal recordings.

Hypersynchronous network states are a continuum bridging interictal and ictal network states.
Analysis of interictal recordings revealed frequent mini-seizure occurrences across the patient cohort (**Figure 6**). In representative examples from two patients (Panel A), mini-seizures occurred repeatedly during brief interictal periods, with distinct temporal patterns unique to each patient. Quantitative analysis across our cohort of 159 patients demonstrated a consistent presence of mini-seizures, with a median occurrence rate of 5.8 events per minute (Panel B). Notably, examination of longer recording segments (Panel C) revealed an interictal-ictal continuum, where mini-seizure frequency systematically increased leading up to and during clinical seizures. This temporal evolution was observed consistently across patients, as demonstrated in the two representative cases shown. These findings provide evidence that mini-seizures represent a fundamental feature of dynamic epileptic networks, potentially serving as a bridge between interictal and ictal states.

Synchronization network properties follow power-law distributions exhibiting transitions between normal and hypersynchronous network states.
Statistical analysis of synchronization network properties revealed distinct characteristics between normal network state and hypersynchronous network state regimes across multiple metrics (**Figure 7**). The distribution of average giant connected component (GCC) edge weights follows a power law with bimodal regimes, where the mini-seizure regime is characterized by significantly higher edge weights, indicating stronger functional connectivity during these events. Similarly, the Fiedler eigenvalue distribution demonstrated a marked separation between normal and MS states, with MS events showing elevated values reflecting increased network synchronizability. Node degree variance exhibited a comparable pattern, with the MS regime displaying higher variances, suggesting the

emergence of hub-like structures during mini-seizures. Notably, analysis of the temporal dynamics between successive mini-seizures revealed a striking power-law relationship in the inter-mini-seizure intervals, as demonstrated in the log-log plot. This power-law scaling, evident over approximately two orders of magnitude, suggests that mini-seizures follow a scale-free temporal organization characteristic of self-organized critical systems. The linear relationship in the log-log plot extends from sub-second to approximately 10-second intervals, beyond which the relationship deviates from power-law behavior, potentially indicating a transition to different dynamical regimes at longer timescales.

HiSyncDx-based EZ identification model accurately predicts the EZ, with ripple band networks being the most discriminative.

HiSyncDx-based EZ prediction model demonstrated robust performance across multiple temporal scales and feature sets. With full-length iEEG recordings (5 minutes - 90 minutes), the model achieved exceptional performance in predicting the EZ (the SOZ within the resected brain reigons) with an F1 score > 95% and maintained its strong performance even with reduced recording durations (F1 score > 90%), demonstrating the robustness of the model. The feature importance analysis in the space of the frequency bands revealed that the ripple band is crucial to the prediction power of the model, as there is a sharp decline in the F1 score when the ripple band is dropped in the HiSyncDx network construction. Analogously, in the summary statistics domain, kurtosis captures the most informative description of the HiSyncDx network dynamics, which is critical for accurate EZ identification. These findings underscore the importance of capturing complex statistical properties of ripple-band activity for accurate EZ identification.

HiSyncDx-based EZ prediction model can accurately delineate EZ from interictal iEEG segments with a duration as short as 3 minutes.

Analysis of EZ likelihood scores across different recording durations revealed that brief interictal segments are sufficient to identify EZ which are critical for surgical success. We observed consistent EZ prediction patterns across recording durations ranging from 1 to 90 minutes, with stable identification of high-likelihood EZ channels emerging by 3 minutes of iEEG recording. Patient 1, who achieved seizure freedom, showed strong alignment between the resection margin and channels with high EZ centrality scores. In contrast, Patients 2 and 3, who did not achieve seizure freedom, exhibited high EZ likelihood scores in channels outside their respective resection margins, suggesting incomplete removal of epileptogenic tissue. The spatial distribution of EZ likelihood scores, when mapped onto brain reconstructions, revealed distinct contiguous hotspots representing potential epileptogenic foci. This spatial organization was particularly evident in Patient 1, where the resected region encompassed

all identified hotspots, correlating with the favorable outcome. Notably, in Patients 2 and 3, the presence of high-likelihood EZ regions outside the resection margin (visible in both heatmaps and brain reconstructions) corresponded with continued seizures, validating the clinical relevance of our prediction model. These findings suggest that HiSyncDx can reliably identify critical epileptogenic regions from short interictal recordings, potentially improving surgical planning and outcome prediction.

HiSyncDx-based surgical outcome prediction model outperforms the state-of-the-art performance

The seizure freedom probability (Ps) score, as outputted by the HiSyncDx-based surgical outcome prediction model, is significantly different (two-sample t-test, $p < 10^{-3}$) between the two groups with seizure-free group consistently having higher predictive values (mean = 0.77, variance = 0.08) than the non-seizure free group (mean = 0.48, variance = 0.14) reflecting the predictive power of the model. Also, the prediction model has robust generalization capability as shown by the strong performance metrics with notably low variance: F1 score (mean = 0.87, variance = 0.004), accuracy (mean = 0.80, variance = 0.009), precision (mean = 0.83, variance = 0.005), and particularly high recall (mean = 0.92, variance = 0.007). Finally, our prediction model (mean F1 score = 87%) significantly outperformed both the HFO-based model (mean F1 score = 79%) and the current clinical standard using SOZ resection status (mean F1 score = 78%) across all performance metrics.

DISCUSSION:

In this study, we developed the HiSyncDx platform to model dynamic and complex epileptic networks in 159 patients with focal drug-resistant epilepsy who underwent iEEG monitoring. We found that frequent hypersynchronous events utilize the regions around the SOZ as hubs. Using a data-driven approach based on network properties, we defined these hypersynchronous events as mini-seizures. The temporal dynamics of mini-seizures revealed a striking power-law relationship in the inter-mini-seizure intervals. We then demonstrated that our prediction model, which incorporates hypersynchronous network properties along with clinical information (such as SOZ location), successfully identifies EZ hubs. Furthermore, when factoring in the resection status of the EZ hubs, the model accurately predicted postoperative seizure outcomes at one year.

Mini-seizures as novel interictal iEEG Biomarker of the EZ.

Our findings are clinically important since no spatial biomarker of the EZ is available, especially when using short iEEG data. Our new framework suggests that mini-seizures and seizures are both part of the same continuum of synchronization events that are generated by the pathophysiology dynamics of epilepsy.[27] We have provided evidence that instead of waiting 1-2 weeks to capture large

events (seizures), capturing frequently occurring mini-seizures provides necessary information regarding which brain regions should be targeted for resection or disruption. This finding represents a significant potential paradigm shift in clinical practice. Historically, clinicians have relied on expert identification of EEG patterns, focusing on EEG channel-based regions and defining several different event annotations. For example, interictal high-frequency oscillations (HFOs) have emerged as a promising biomarker of the EZ.[40-45] HFOs represent pathological bursts of neuronal activity that occur in the frequency range of 80-500 Hz, generated by the epileptogenic brain tissues.[46-48] Interictal HFOs were observed around the SOZ, and retrospective studies demonstrated that resection of HFO-generating regions correlated with favorable postoperative seizure outcomes.[40, 44, 49-52] However, this optimism has been tempered by conflicting evidence from more recent observational studies, which failed to confirm the utility of HFOs in predicting postoperative seizure outcomes.[53, 54] A clinical trial failed to prove that HFO-guided resection would improve postoperative seizure outcomes compared to standard, spike-guided resection during intraoperative electrocorticography.[55] One major limitation is that HFOs can occur in healthy brain regions,[32, 56, 57] leading to false positives. Also, the detection of HFOs typically relies on algorithms applied independently to each channel, overlooking the broader concept of regional network dynamics. Network properties, such as propagation in spike[58] and HFO analysis,[59] have been shown to enhance the prediction of the EZ. However, these methods remain constrained by the requirement to first detect spikes or HFOs in each channel as an initial step, which limits their applicability. Our proposed framework fundamentally shifts the paradigm of epilepsy surgery from the traditional approach of estimating the EZ through expert-annotated discrete regions, such as the SOZ, to a network-based approach. HiSyncDx employs a data-driven strategy to identify EZ hubs and target them for resection or disruption, preventing the perturbed network from generating hyper-synchronous states and ultimately eliminating seizures.

The HiSyncDx platform provides a more comprehensive network analysis than prior methods.

Our conceptual hypothesis of mini-seizures and seizures being part of a continuum of synchronization events is based on a shared behavior exhibited by most bursty complex dynamical systems, where a stream of smaller events of varying magnitudes occur continually and as an integral part of the same continuum of events, rare large events occur that are felt throughout the system.[24-31] For example, around active fault zones in the earth's crusts, small micro-earthquakes occur continually; larger earthquakes felt over a wide area are a natural part of this continuum.[60, 61] Thus, micro and large earthquakes occur because of the same shared dynamics around a fault system. Epileptic seizures arise from the dynamic interplay between excitatory and inhibitory neurophysiological processes at neuronal, local circuit, regional, and whole brain levels.[15, 62, 63] In the EZ, this balance is disrupted, leading to clusters of neurons that often fire pathologically at higher frequencies.[64] Thus, we

hypothesize and validate that the EZ continually produces synchronization events of various magnitudes. Moreover, just as in the case of earthquakes, the geometry of fault zones and their stress distributions are routinely mapped via naturally occurring and induced micro-quakes without having to wait for larger quakes.[65, 66] We are showing that the EZ can be similarly and accurately estimated from the mini-seizures that occur in randomly picked short interictal periods.

As articulated in this work, HiSyncDx uses a novel data-driven algorithm capable of analyzing large-scale, non-linear complex systems. By applying graph theory and inferring connections of networks (ICON) methodology[39] on iEEG data, the HiSyncDx platform provides a (1) comprehensive spatial characterization of complex epileptic networks and (2) detection of their dynamic temporal evolution within a timeframe of approximately hundreds of milliseconds. Specifically, the HiSyncDx framework evaluates each node, representing a specific brain region, and quantifies its ability to drive high-frequency synchronization events, measured as the EZ centrality score. Similarly, each edge is quantified by the strength and direction of network synchronization between corresponding regions. These spatial characteristics of network synchronization can then be analyzed with a temporal resolution of hundreds of milliseconds, providing a significant advantage over other methods, such as fMRI, which typically has a temporal resolution of 1-3 seconds. Once trained with machine learning algorithms, the platform's efficient parallel computation capabilities will enable deployment on lightweight platforms, allowing it to run on personal computers for both research and clinical applications.

Although numerous studies on animal models and human research using neuroimaging and neurophysiology have demonstrated epilepsy involves network pathology, no comprehensive network analysis platform such as HiSyncDx has been proposed to date. Although the source-sink theory is compelling, its methodologies face limitations in capturing key neurophysiological aspects of epilepsy network dynamics. A "sink" node is defined as a region highly influenced by other nodes but not influential itself. In contrast, a "source" node is defined as a region in the brain network that is highly influential towards other nodes but is not being influenced by others. Thus, the EZ acts as a sink node that is persistently inhibited by neighboring source nodes during interictal periods. Using the source-sink theory, recent studies investigated epilepsy patients using a multimodal approach, combining diffusion MRI to assess structural connectivity and resting SEEG to quantify functional connectivity, which demonstrated improved identification of the SOZ.[20] Other studies applied graph theory-based connectivity analysis to iEEG data, including interictal and pre-ictal/ictal periods, to identify hubs within epileptic networks.[64, 67] The resection status of the network hubs contributed to predicting postoperative seizure outcomes. Such studies have succeeded in determining the "sink" status of the EZ over the duration of 5-20 minutes of the interictal iEEG segment. However, their linear connectivity analysis

methods[20, 21] make it difficult to describe dynamic transitions of the epileptic network across interictal, preictal, and ictal states. More specifically, the prior research overlooked rapid synchronization changes that could resemble seizures within the short iEEG segment (mini-seizures). Also, the "sink" status reflects the baseline state of the channels, but capturing their active "source" state—which more closely represents the ictal state—within interictal iEEG data may provide a more accurate delineation of the EZ hubs. Although neural fragility theory[64] effectively models the unstable transition from the pre-ictal to ictal state within SOZ using a time-varying linear model, the methodology is limited by the need for ictal EEG data for model training. Besides, this method is not meant to model overall non-linear, non-stationary interictal-ictal dynamics across the iEEG recording.

Limitations and further perspectives

While our findings are promising, several limitations should be acknowledged. This study relied on macroelectrode recordings, which may not fully capture fine-grained neurophysiological mechanisms at the single-neuron level. A more comprehensive characterization of multidimensional network states—spanning cellular, local, and regional brain levels—may require integrating both micro- and macroelectrode recordings. Also, our analysis focused on pediatric epilepsy with neocortical seizure onsets, utilizing only iEEG recordings from subdural grids. Expanding this work to include stereotactic EEG and adult epilepsy populations would provide broader insights. Finally, validating our approach based on clinical outcomes remains crucial. Evaluating seizure outcomes following neuromodulation, rather than resection alone, would be a meaningful next step in confirming the clinical utility of our findings. Although we demonstrated that a five-minute iEEG segment is sufficient to detect mini-seizures in each patient, longer multi-day recordings could provide further insights into the temporal dynamics of mini-seizure occurrence.[68] Additionally, the influence of vigilance states should be considered,[69] as differences in mini-seizure morphology across sleep stages and wakefulness remain underexplored. Despite these limitations, our publicly available data and analysis code allow other research groups to validate our findings. Looking ahead, we plan to integrate iEEG data with non-invasive EEG and neuroimaging modalities[70] to enhance our understanding of epileptic networks. Moreover, collaborating with additional institutions will be crucial to test the generalizability of our approach.

ACKNOWLEDGMENTS

HN is supported by the National Institute of Neurological Disorders and Stroke (NINDS) K23NS128318, the Sudha Neelakantan & Venky Harinarayan Charitable Fund, the Elsie and Isaac Fogelman Endowment, and the UCLA Children’s Discovery and Innovation Institute (CDI) Junior Faculty Career Development Grant (#CDI-SEED-010124). AD is supported by the Uehara Memorial Foundation and

the SENSHIN Medical Research Foundation. EA is supported by the National Institute of Health (R01NS064033). The research described was also supported by NIH/National Center for Advancing Translational Science (NCATS) UCLA CTSI Grant Number UL1TR001881. The authors have no conflict of interest to disclose. We confirm that we have read the Journal's position on issues involved in ethical publication and a□rm that this report is consistent with those guidelines.

FIGURE LEGENDS

Fig. 1: Overview of HiSyncDx network construction.

Fig. 2: Overview of HiSyncDx-based EZ prediction.

Fig. 3: Development of HiSyncDx-based postoperative seizure outcomes prediction.

Fig. 4: HiSyncDx can detect hypersynchronous states in both interictal and ictal EEG segments. In the interictal state (A), transient hypersynchronous states (mini-seizures) emerge, involving the SOZ and resembling ictal network patterns. During ictal periods (B), the hypersynchronous state, with similar functional connections and pathophysiology, emerges at the ictal onset. The weighted adjacency matrices heatmap demonstrates these transient hypersynchronous events, with warmer colors indicating stronger functional connections between electrode pairs.

Fig. 5: A data-driven definition of mini-seizures. (A) Local and global node characteristics difference between normal and hypersynchronous network states. (B) With the distribution of the synchronization index (Fiedler Eigenvalue * Average GCC edge weight * Node degree variance), the mini-seizure threshold was defined. Note habitual seizures exhibited a larger synchronization index than mini-seizures.

Fig. 6: HiSyncDx detects frequently occurring mini-seizures, encompassing actual ictal events. (A) Representative examples from two patients demonstrating frequent mini-seizures within brief interictal iEEG recordings. (B) Box plot illustrating the distribution of mini-seizure occurrence rates (median 5.8 per minute). (C) Examples from two patients exhibiting an interictal-ictal continuum, where the frequency of synchronization events increases during ictal events. Blue dots represent high-frequency oscillations (HFOs) with spikes. Temporal locations of such pathological HFOs are generally matched with corresponding mini-seizures, implying a strong pathological origin of mini-seizures themselves. Many mini-seizure events, however, do not have corresponding HFOs with spikes. Thus, interictal mini-seizures are a more sensitive indicator of the EZ than pathological HFOs.

Fig. 7: Statistical characterization of mini-seizure dynamics reveals distinct network states and power-law behavior. Complex dynamical systems are characterized by scaling laws (ref. simkin+roychowdhury) that govern the distributions of key macroscopic metrics. Several key global metrics of the hypersynchronous synchronization networks, including its Fiedler eigenvalue, average synchronization edge weights, and node degree variance, show linear trends in log-log plots. Moreover, the distributions of these metrics for mini-seizure and ictal networks show a distinctly different trend from that of the baseline normal activity networks. Similarly, just as with earthquakes, the distribution of the inter-mini-seizure intervals shows a distinct power-law distribution, which is a trademark critical behavior shown by most complex dynamical systems.

Fig. 8: HiSyncDx-based EZ prediction model accurately predicts SOZ status, with ripple band features being the most informative. A leave-one-out cross-validation approach was used to validate the performance of the model. The X-axis represents the four performance metrics, and Y-axis represents the value of the performance metric averaged across 159 patients with an error bar showing the variance. The model using all frequency bands generalizes well, as shown by the high average F1 score of 0.97 and small variance in F1 score across 159 patients. However, when the ripple frequency band was dropped, the model performance decreased significantly to an average F1 score of 0.84, showing the importance of the ripple band in SOZ classification.

Fig. 9: Short interictal iEEG segments are sufficient for high-confidence EZ identification. Heatmaps of EZ centrality scores for three patients are shown with rows representing the channels and columns representing the duration of the iEEG epoch used to train/test the EZ classification model. A patient whose resection margins included all the predicted EZ became seizure-free (left). Conversely, patients whose resection margin did not cover all the channels with predicted EZ did not become seizure-free (middle and right). Note that the resection margin includes the two identified SOZ channels in the patient represented in the right figure. The preserved region, however, includes a number of predicted EZ channels that were not annotated as SOZ; not resecting such EZ hubs most likely contributed to the failure of surgical intervention.

Fig. 10: Network-based model accurately predicts postoperative seizure outcome. A 10-fold cross-validation (CV) approach was used to validate the performance of the surgical outcome prediction models. (A) The synchronization network-based model outputs a seizure freedom probability (Ps) for each patient. Each dot represents one patient, and the dots are color-coded according to the surgical outcome. For the network-based model, the majority of patients with a successful surgical

outcome (red dots) had Ps values greater than the threshold (dotted line), whereas patients with a failed surgical outcome generally had Ps values below the threshold. (B) Box plots show distributions of each performance metric across the 10 CV folds. The network-based model generalizes well, as shown by the high mean F1 score of 0.87 and low variance of 0.004 across the 10 CV folds. (C) Four surgical outcome prediction models are compared in terms of 4 performance metrics. The synchronization network-based model (mean F1 score - 87%) outperforms the HFO-based model (mean F1 score - 79%) and SOZ resection status-based model (current clinical standard) (mean F1 score - 78%) on all four performance metrics.

REFERENCES

1. Hauser WA. 1994. 'The prevalence and incidence of convulsive disorders in children', *Epilepsia*, 35 Suppl 2: S1-6.
2. 2019. 'Global, regional, and national burden of neurological disorders, 1990-2016: a systematic analysis for the Global Burden of Disease Study 2016', *Lancet Neurol*, 18: 459-480. PMC6459001
3. Kwan P, Brodie MJ. 2000. 'Early identification of refractory epilepsy', *N Engl J Med*, 342: 314-319.
4. Sillanpää M, Shinnar S. 2010. 'Long-term mortality in childhood-onset epilepsy', *N Engl J Med*, 363: 2522-2529.
5. Engel J, Jr. 2016. 'What can we do for people with drug-resistant epilepsy? The 2016 Wartenberg Lecture', *Neurology*, 87: 2483-2489. PMC5177675
6. Zhang L, Hall M, Lam SK. 2023. 'Comparison of long-term survival with continued medical therapy, vagus nerve stimulation, and cranial epilepsy surgery in paediatric patients with drug-resistant epilepsy in the USA: an observational cohort study', *Lancet Child Adolesc Health*, 7: 455-462.
7. Widjaja E, Puka K, Speechley KN, Ferro MA, Connolly MB, Major P, Gallagher A, Almubarak S, Hasal S, Ramachandrannair R, Andrade A, Xu Q, Leung E, Snead OC, 3rd, Smith ML. 2023. 'Trajectory of Health-Related Quality of Life After Pediatric Epilepsy Surgery', *JAMA Netw Open*, 6: e234858. PMC10043749
8. Rosenow F, Luders H. 2001. 'Presurgical evaluation of epilepsy', *Brain*, 124: 1683-1700.
9. Cardinale F, Rizzi M, Vignati E, Cossu M, Castana L, d'Orio P, Revay M, Costanza MD, Tassi L, Mai R, Sartori I, Nobili L, Gozzo F, Pelliccia V, Mariani V, Lo Russo G, Francione S. 2019. 'Stereoelectroencephalography: retrospective analysis of 742 procedures in a single centre', *Brain*, 142: 2688-2704.
10. Jayakar P, Gotman J, Harvey AS, Palmini A, Tassi L, Schomer D, Dubeau F, Bartolomei F, Yu A, Kršek P, Velis D, Kahane P. 2016. 'Diagnostic utility of invasive EEG for epilepsy surgery: Indications, modalities, and techniques', *Epilepsia*, 57: 1735-1747.
11. Asano E, Juhasz C, Shah A, Sood S, Chugani HT. 2009. 'Role of subdural electrocorticography in prediction of long-term seizure outcome in epilepsy surgery', *Brain*, 132: 1038-1047. PMC2668945
12. Cuello Oderiz C, von Ellenrieder N, Dubeau F, Eisenberg A, Gotman J, Hall J, Hincapié AS, Hoffmann D, Job AS, Khoo HM, Minotti L, Olivier A, Kahane P, Frauscher B. 2019. 'Association of Cortical Stimulation-Induced Seizure With Surgical Outcome in Patients With Focal Drug-Resistant Epilepsy', *JAMA Neurol*, 76: 1070-1078. PMC6563597
13. Widjaja E, Jain P, Demoe L, Guttmann A, Tomlinson G, Sander B. 2020. 'Seizure outcome of pediatric epilepsy surgery: Systematic review and meta-analyses', *Neurology*, 94: 311-321.
14. Kramer MA, Cash SS. 2012. 'Epilepsy as a disorder of cortical network organization', *Neuroscientist*, 18: 360-372. PMC3736575
15. Scott RC, Menendez de la Prida L, Mahoney JM, Kobow K, Sankar R, de Curtis M. 2018. 'WONOEP APPRAISAL: The many facets of epilepsy networks', *Epilepsia*, 59: 1475-1483.
16. Johnson GW, Doss DJ, Englot DJ. 2022. 'Network dysfunction in pre and postsurgical epilepsy: connectomics as a tool and not a destination', *Current Opinion in Neurology*, 35: 196-201. PMC8891078

17. Blumenfeld H. 2005. 'Cellular and network mechanisms of spike-wave seizures', *Epilepsia*, 46 Suppl 9: 21-33.
18. Blumenfeld H, Varghese GI, Purcaro MJ, Motelow JE, Enev M, McNally KA, Levin AR, Hirsch LJ, Tikofsky R, Zubal IG, Paige AL, Spencer SS. 2009. 'Cortical and subcortical networks in human secondarily generalized tonic-clonic seizures', *Brain*, 132: 999-1012. PMC2724910
19. Burns SP, Santaniello S, Yaffe RB, Jouny CC, Crone NE, Bergey GK, Anderson WS, Sarma SV. 2014. 'Network dynamics of the brain and influence of the epileptic seizure onset zone', *Proc Natl Acad Sci U S A*, 111: E5321-5330. PMC4267355
20. Johnson GW, Doss DJ, Morgan VL, Paulo DL, Cai LY, Shless JS, Negi AS, Gummadavelli A, Kang H, Reddy SB, Naftel RP, Bick SK, Williams Roberson S, Dawant BM, Wallace MT, Englot DJ. 2023. 'The Interictal Suppression Hypothesis in focal epilepsy: network-level supporting evidence', *Brain*, 146: 2828-2845. PMC10316780
21. Englot DJ, Hinkley LB, Kort NS, Imber BS, Mizuiri D, Honma SM, Findlay AM, Garrett C, Cheung PL, Mantle M, Tarapore PE, Knowlton RC, Chang EF, Kirsch HE, Nagarajan SS. 2015. 'Global and regional functional connectivity maps of neural oscillations in focal epilepsy', *Brain*, 138: 2249-2262. PMC4840946
22. Akbarian B, Sainburg LE, Janson A, Johnson G, Doss DJ, Rogers BP, Englot DJ, Morgan VL. 2024. 'Association Between Postsurgical Functional Connectivity and Seizure Outcome in Patients With Temporal Lobe Epilepsy', *Neurology*, 103: e209816. PMC11373675 disclosures.
23. Morgan VL, Rogers BP, González HFJ, Goodale SE, Englot DJ. 2020. 'Characterization of postsurgical functional connectivity changes in temporal lobe epilepsy', *Journal of Neurosurgery*, 133: 392-402. PMC6911037
24. Farazmand M, Sapsis TP. 2019. 'Extreme events: Mechanisms and prediction', *Applied Mechanics Reviews*, 71: 050801.
25. Mishra A, Leo Kingston S, Hens C, Kapitaniak T, Feudel U, Dana SK. 2020. 'Routes to extreme events in dynamical systems: Dynamical and statistical characteristics', *Chaos*, 30: 063114.
26. Simkin M, Roychowdhury V. 2008. 'A theory of web traffic', *Europhysics Letters*, 82: 28006.
27. Simkin M, Roychowdhury V. 2010. 'An explanation of the distribution of inter-seizure intervals', *Europhysics Letters*, 91: 58005.
28. Simkin MV, Roychowdhury VP. 2011. 'Re-inventing willis', *Physics Reports*, 502: 1-35.
29. Simkin M, Roychowdhury V. 2014. 'Stochastic modeling of a serial killer', *Journal of Theoretical Biology*, 355: 111-116.
30. Miyahara H, Qian H, Holur PS, Roychowdhury V. 2024. 'Emergent invariance and scaling properties in the collective return dynamics of a stock market', *PloS One*, 19: e0298789.
31. Sarshar N, Roychowdhury V. 2004. 'Scale-free and stable structures in complex ad hoc networks', *Physical Review E*, 69: 026101.
32. Kuroda N, Sonoda M, Miyakoshi M, Nariai H, Jeong JW, Motoi H, Luat AF, Sood S, Asano E. 2021. 'Objective interictal electrophysiology biomarkers optimize prediction of epilepsy surgery outcome', *Brain Commun*, 3: fcab042. PMC8088817
33. Zhang Y, Lu Q, Monsoor T, Hussain SA, Qiao JX, Salamon N, Fallah A, Sim MS, Asano E, Sankar R, Staba RJ, Engel J, Jr., Speier W, Roychowdhury V, Nariai H. 2022. 'Refining epileptogenic high-frequency oscillations using deep learning: a reverse engineering approach', *Brain Commun*, 4: fcab267. PMC8833577
34. Fischl B. 2012. 'FreeSurfer', *Neuroimage*, 62: 774-781. PMC3685476
35. Klein A, Tourville J. 2012. '101 labeled brain images and a consistent human cortical labeling protocol', *Frontiers in Neuroscience*, 6: 171. PMC3514540
36. Tadel F, Baillet S, Mosher JC, Pantazis D, Leahy RM. 2011. 'Brainstorm: a user-friendly application for MEG/EEG analysis', *Computational Intelligence and Neuroscience*, 2011: 879716. PMC3090754

37. Wu J, Ngo GH, Greve D, Li J, He T, Fischl B, Eickhoff SB, Yeo BTT. 2018. 'Accurate nonlinear mapping between MNI volumetric and FreeSurfer surface coordinate systems', *Hum Brain Mapp*, 39: 3793-3808. PMC6239990
38. Nariai H, Hussain SA, Bernardo D, Fallah A, Murata KK, Nguyen JC, Rajaraman RR, Rao LM, Matsumoto JH, Lerner JT, Salamon N, Elashoff D, Sankar R, Wu JY. 2019. 'Prospective observational study: Fast ripple localization delineates the epileptogenic zone', *Clin Neurophysiol*, 130: 2144-2152.
39. Wang S, Herzog ED, Kiss IZ, Schwartz WJ, Bloch G, Sebek M, Granados-Fuentes D, Wang L, Li JS. 2018. 'Inferring dynamic topology for decoding spatiotemporal structures in complex heterogeneous networks', *Proc Natl Acad Sci U S A*, 115: 9300-9305. PMC6140519
40. Worrell GA, Parish L, Cranstoun SD, Jonas R, Baltuch G, Litt B. 2004. 'High-frequency oscillations and seizure generation in neocortical epilepsy', *Brain*, 127: 1496-1506.
41. Jirsch JD, Urrestarazu E, LeVan P, Olivier A, Dubeau F, Gotman J. 2006. 'High-frequency oscillations during human focal seizures', *Brain*, 129: 1593-1608.
42. Staba RJ, Wilson CL, Bragin A, Fried I, Engel J, Jr. 2002. 'Quantitative analysis of high-frequency oscillations (80-500 Hz) recorded in human epileptic hippocampus and entorhinal cortex', *Journal of Neurophysiology*, 88: 1743-1752.
43. Zijlmans M, Jacobs J, Zelmann R, Dubeau F, Gotman J. 2009. 'High-frequency oscillations mirror disease activity in patients with epilepsy', *Neurology*, 72: 979-986. Pmc3797085
44. Urrestarazu E, Chander R, Dubeau F, Gotman J. 2007. 'Interictal high-frequency oscillations (100-500 Hz) in the intracerebral EEG of epileptic patients', *Brain*, 130: 2354-2366.
45. Gotman J. 2010. 'High frequency oscillations: the new EEG frontier?', *Epilepsia*, 51 Suppl 1: 63-65. Pmc3786932
46. Bragin A, Engel J, Jr., Wilson CL, Fried I, Mathern GW. 1999. 'Hippocampal and entorhinal cortex high-frequency oscillations (100--500 Hz) in human epileptic brain and in kainic acid--treated rats with chronic seizures', *Epilepsia*, 40: 127-137.
47. Bragin A, Engel J, Jr., Wilson CL, Vizentin E, Mathern GW. 1999. 'Electrophysiologic analysis of a chronic seizure model after unilateral hippocampal KA injection', *Epilepsia*, 40: 1210-1221.
48. Bragin A, Mody I, Wilson CL, Engel J, Jr. 2002. 'Local generation of fast ripples in epileptic brain', *J Neurosci*, 22: 2012-2021.
49. Jacobs J, Zijlmans M, Zelmann R, Chatillon CE, Hall J, Olivier A, Dubeau F, Gotman J. 2010. 'High-frequency electroencephalographic oscillations correlate with outcome of epilepsy surgery', *Ann Neurol*, 67: 209-220. Pmc3769290
50. Wu JY, Sankar R, Lerner JT, Matsumoto JH, Vinters HV, Mathern GW. 2010. 'Removing interictal fast ripples on electrocorticography linked with seizure freedom in children', *Neurology*, 75: 1686-1694. Pmc3033604
51. Akiyama T, McCoy B, Go CY, Ochi A, Elliott IM, Akiyama M, Donner EJ, Weiss SK, Snead OC, 3rd, Rutka JT, Drake JM, Otsubo H. 2011. 'Focal resection of fast ripples on extraoperative intracranial EEG improves seizure outcome in pediatric epilepsy', *Epilepsia*, 52: 1802-1811.
52. Worrell GA, Gardner AB, Stead SM, Hu S, Goerss S, Cascino GJ, Meyer FB, Marsh R, Litt B. 2008. 'High-frequency oscillations in human temporal lobe: simultaneous microwire and clinical macroelectrode recordings', *Brain*, 131: 928-937. Pmc2760070
53. Jacobs J, Wu JY, Perucca P, Zelmann R, Mader M, Dubeau F, Mathern GW, Schulze-Bonhage A, Gotman J. 2018. 'Removing high-frequency oscillations: A prospective multicenter study on seizure outcome', *Neurology*, 91: e1040-e1052. PMC6140372
54. Roehri N, Pizzo F, Lagarde S, Lambert I, Nica A, McGonigal A, Giusiano B, Bartolomei F, Benar CG. 2018. 'High-frequency oscillations are not better biomarkers of epileptogenic tissues than spikes', *Ann Neurol*, 83: 84-97.
55. Zweiphenning W, Klooster MAV, van Klink NEC, Leijten FSS, Ferrier CH, Gebbink T, Huiskamp G, van Zandvoort MJE, van Schooneveld MMJ, Bourez M, Goemans S, Straumann S, van Rijen PC, Gosselaar PH, van Eijsden P, Otte WM, van Diessen E, Braun KPJ, Zijlmans M. 2022.

'Intraoperative electrocorticography using high-frequency oscillations or spikes to tailor epilepsy surgery in the Netherlands (the HFO trial): a randomised, single-blind, adaptive non-inferiority trial', *Lancet Neurol*, 21: 982-993. PMC9579052

56. Frauscher B, von Ellenrieder N, Zelmann R, Rogers C, Nguyen DK, Kahane P, Dubeau F, Gotman J. 2018. 'High-Frequency Oscillations in the Normal Human Brain', *Ann Neurol*, 84: 374-385.
57. Guragain H, Cimbalnik J, Stead M, Groppe DM, Berry BM, Kremen V, Kenney-Jung D, Britton J, Worrell GA, Brinkmann BH. 2018. 'Spatial variation in high-frequency oscillation rates and amplitudes in intracranial EEG', *Neurology*, 90: e639-e646. PMC5818159
58. Matarrese MAG, Loppini A, Fabbri L, Tamilia E, Perry MS, Madsen JR, Bolton J, Stone SSD, Pearl PL, Filippi S, Papadelis C. 2023. 'Spike propagation mapping reveals effective connectivity and predicts surgical outcome in epilepsy', *Brain*, 146: 3898-3912. PMC10473571
59. Tamilia E, Park EH, Percivati S, Bolton J, Taffoni F, Peters JM, Grant PE, Pearl PL, Madsen JR, Papadelis C. 2018. 'Surgical resection of ripple onset predicts outcome in pediatric epilepsy', *Ann Neurol*, 84: 331-346.
60. Nadeau RM, Foxall W, McEvilly TV. 1995. 'Clustering and periodic recurrence of microearthquakes on the san andreas fault at parkfield, california', *Science*, 267: 503-507.
61. Stabile TA, Satriano C, Orefice A, Festa G, Zollo A. 2012. 'Anatomy of a microearthquake sequence on an active normal fault', *Scientific Reports*, 2: 410. PMC3353283
62. Khoshkhoo S, Vogt D, Sohal VS. 2017. 'Dynamic, Cell-Type-Specific Roles for GABAergic Interneurons in a Mouse Model of Optogenetically Inducible Seizures', *Neuron*, 93: 291-298. PMC5268075
63. Elahian B, Lado NE, Mankin E, Vangala S, Misra A, Moxon K, Fried I, Sharan A, Yeasin M, Staba R, Bragin A, Avoli M, Sperling MR, Engel J, Jr., Weiss SA. 2018. 'Low-voltage fast seizures in humans begin with increased interneuron firing', *Ann Neurol*, 84: 588-600. PMC6814155
64. Li A, Huynh C, Fitzgerald Z, Cajigas I, Brusko D, Jagid J, Claudio AO, Kanner AM, Hopp J, Chen S, Haagensen J, Johnson E, Anderson W, Crone N, Inati S, Zaghloul KA, Bulacio J, Gonzalez-Martinez J, Sarma SV. 2021. 'Neural fragility as an EEG marker of the seizure onset zone', *Nature Neuroscience*, 24: 1465-1474. PMC8547387
65. Terakawa T, Miller SA, Deichmann N. 2012. 'High fluid pressure and triggered earthquakes in the enhanced geothermal system in Basel, Switzerland', *Journal of Geophysical Research: Solid Earth*, 117.
66. Boyd OS, Dreger DS, Gritto R, Garcia J. 2018. 'Analysis of seismic moment tensors and in situ stress during Enhanced Geothermal System development at The Geysers geothermal field, California', *Geophysical Journal International*, 215: 1483-1500.
67. Doss DJ, Shless JS, Bick SK, Makhoul GS, Negi AS, Bibro CE, Rashingkar R, Gummadavelli A, Chang C, Gallagher MJ, Naftel RP, Reddy SB, Williams Roberson S, Morgan VL, Johnson GW, Englot DJ. 2024. 'The interictal suppression hypothesis is the dominant differentiator of seizure onset zones in focal epilepsy', *Brain*, 147: 3009-3017. PMC11370787
68. Gliske SV, Irwin ZT, Chestek C, Hegeman GL, Brinkmann B, Sagher O, Garton HJL, Worrell GA, Stacey WC. 2018. 'Variability in the location of high frequency oscillations during prolonged intracranial EEG recordings', *Nat Commun*, 9: 2155. PMC5984620
69. von Ellenrieder N, Dubeau F, Gotman J, Frauscher B. 2017. 'Physiological and pathological high-frequency oscillations have distinct sleep-homeostatic properties', *Neuroimage Clin*, 14: 566-573. PMC5349616
70. Sun R, Sohrabpour A, Worrell GA, He B. 2022. 'Deep neural networks constrained by neural mass models improve electrophysiological source imaging of spatiotemporal brain dynamics', *Proc Natl Acad Sci U S A*, 119: e2201128119. PMC9351497

Fig. 1

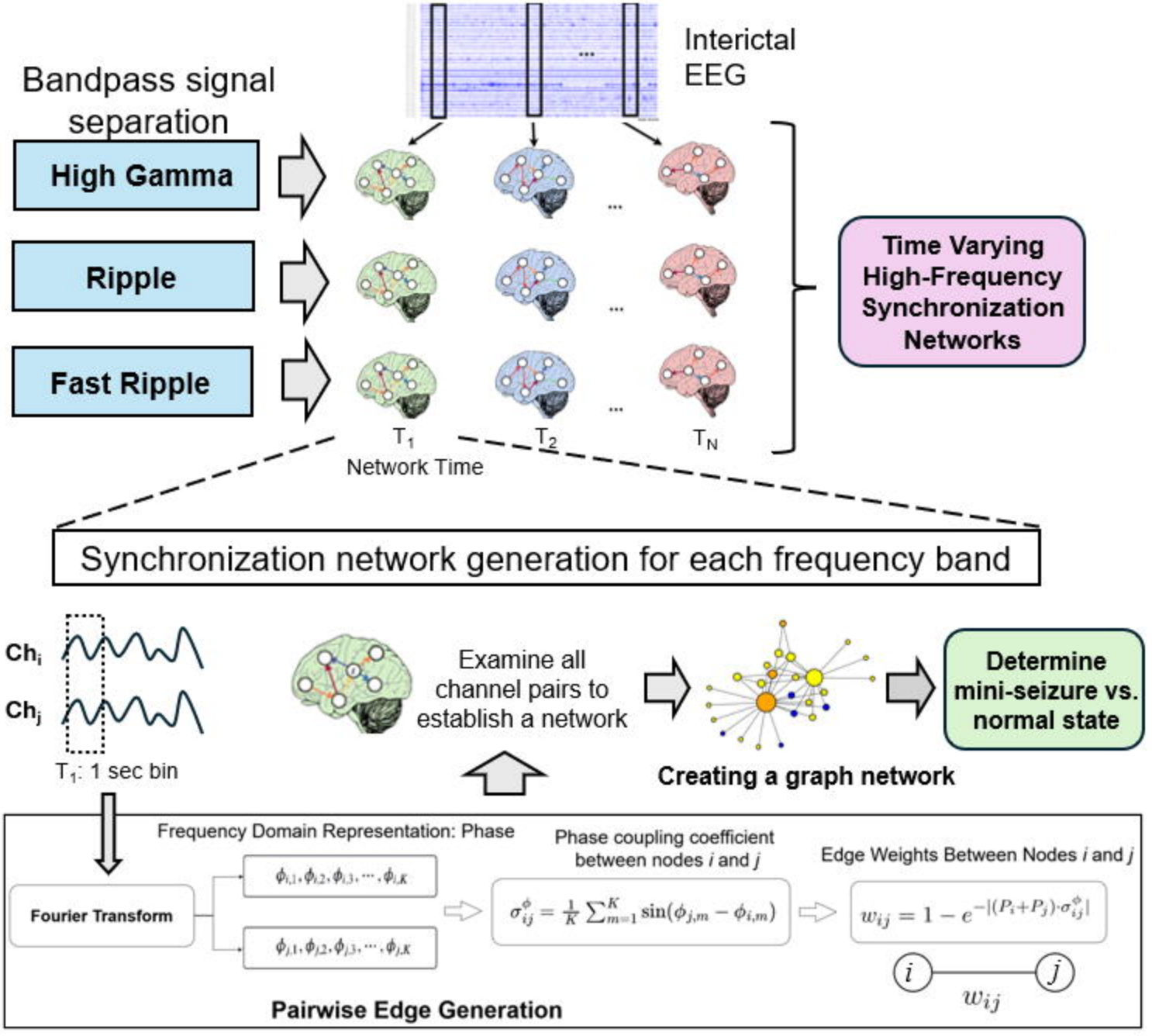
Interictal EEG
Bandpass signal separation
High Gamma
Ripple
Fast Ripple
T1
T2
TN
Network Time
Time Varying High-Frequency Synchronization Networks
Synchronization network generation for each frequency band
Chi
Chj
T1: 1 sec bin
Examine all channel pairs to establish a network
Creating a graph network
Determine mini-seizure vs. normal state
Frequency Domain Representation: Phase
Fourier Transform
$\phi_{i,1}, \phi_{i,2}, \phi_{i,3}, \cdots, \phi_{i,K}$
$\phi_{j,1}, \phi_{j,2}, \phi_{j,3}, \cdots, \phi_{j,K}$
Phase coupling coefficient between nodes i and j
$\sigma_{ij}^{\phi} = \frac{1}{K}\sum_{m=1}^{K}\sin(\phi_{j,m} - \phi_{i,m})$
Edge Weights Between Nodes i and j
$w_{ij} = 1 - e^{-|(P_i+P_j)\cdot\sigma_{ij}^{\phi}|}$
i
j
w_{ij}
Pairwise Edge Generation

Fig. 2

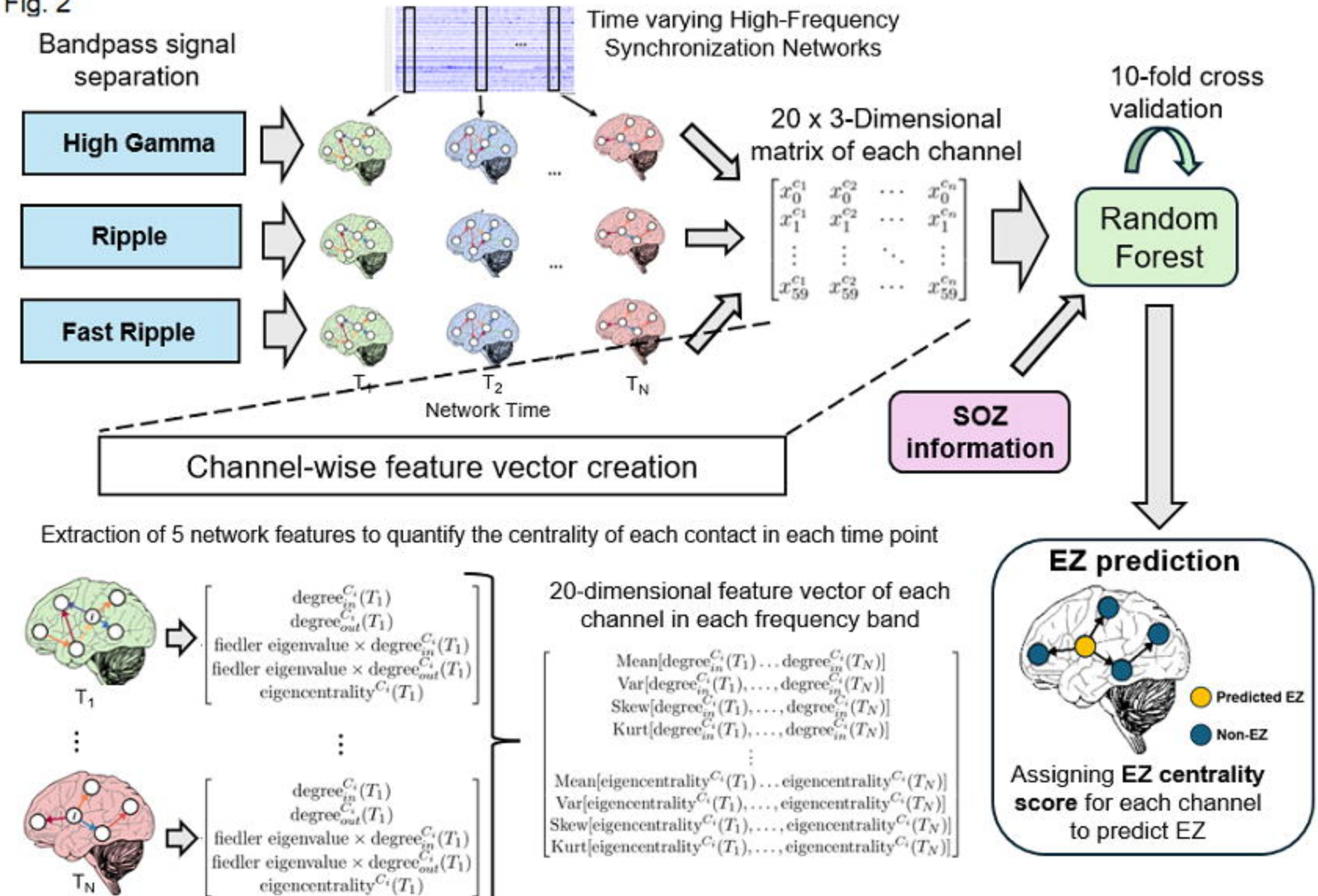
Bandpass signal separation
High Gamma
Ripple
Fast Ripple
Time varying High-Frequency Synchronization Networks
T1
T2
TN
Network Time
20 x 3-Dimensional matrix of each channel
10-fold cross validation
Random Forest
SOZ information
Channel-wise feature vector creation
Extraction of 5 network features to quantify the centrality of each contact in each time point
degree_in^Ci(T1)
degree_out^Ci(T1)
fiedler eigenvalue × degree_in^Ci(T1)
fiedler eigenvalue × degree_out^Ci(T1)
eigencentrality^Ci(T1)
20-dimensional feature vector of each channel in each frequency band
Mean[degree_in^Ci(T1) ... degree_in^Ci(TN)]
Var[degree_in^Ci(T1), ..., degree_in^Ci(TN)]
Skew[degree_in^Ci(T1), ..., degree_in^Ci(TN)]
Kurt[degree_in^Ci(T1), ..., degree_in^Ci(TN)]
Mean[eigencentrality^Ci(T1) ... eigencentrality^Ci(TN)]
Var[eigencentrality^Ci(T1), ..., eigencentrality^Ci(TN)]
Skew[eigencentrality^Ci(T1), ..., eigencentrality^Ci(TN)]
Kurt[eigencentrality^Ci(T1), ..., eigencentrality^Ci(TN)]
EZ prediction
Predicted EZ
Non-EZ
Assigning EZ centrality score for each channel to predict EZ

Fig. 3

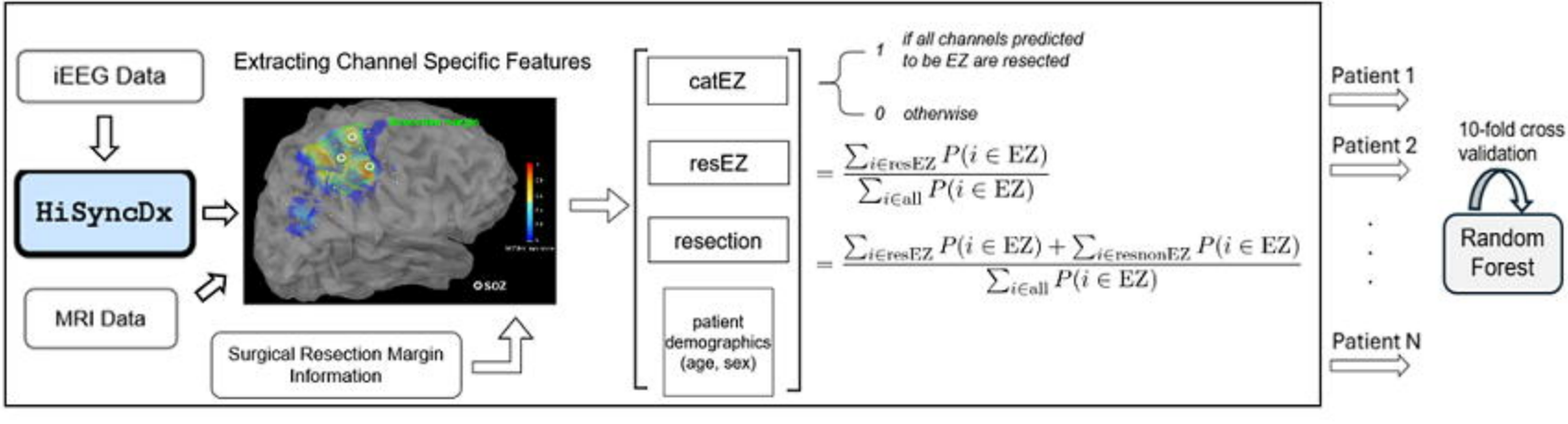
iEEG Data
HiSyncDx
MRI Data
Extracting Channel Specific Features
SOZ
Surgical Resection Margin Information
catEZ
resEZ
resection
patient demographics (age, sex)
1 if all channels predicted to be EZ are resected
0 otherwise
$= \frac{\sum_{i \in \text{resEZ}} P(i \in \text{EZ})}{\sum_{i \in \text{all}} P(i \in \text{EZ})}$
$= \frac{\sum_{i \in \text{resEZ}} P(i \in \text{EZ}) + \sum_{i \in \text{resnonEZ}} P(i \in \text{EZ})}{\sum_{i \in \text{all}} P(i \in \text{EZ})}$
Patient 1
Patient 2
Patient N
10-fold cross validation
Random Forest

Fig. 4

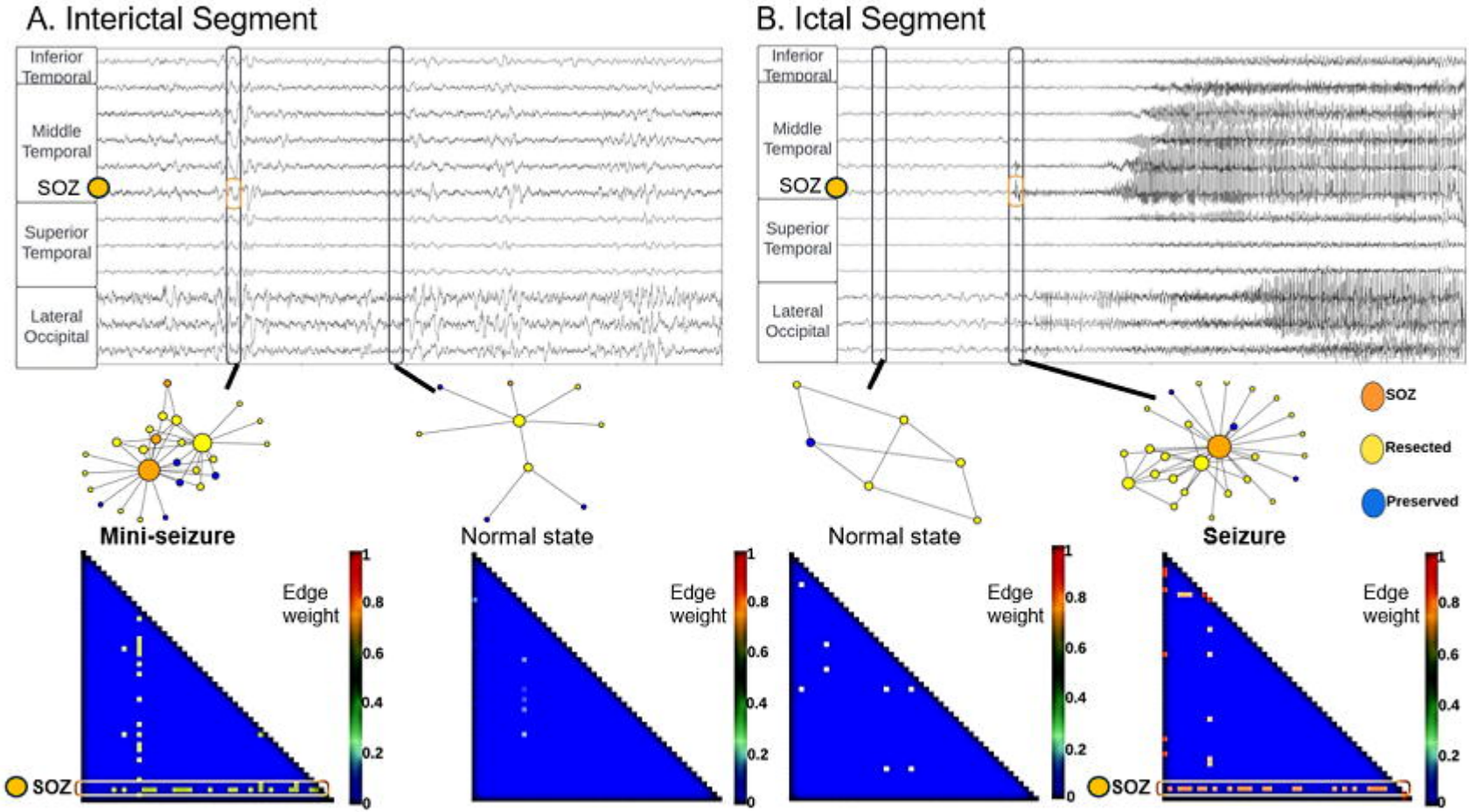
A. Interictal Segment
B. Ictal Segment
Inferior Temporal
Middle Temporal
SOZ
Superior Temporal
Lateral Occipital
Mini-seizure
Normal state
Normal state
Seizure
SOZ
Resected
Preserved
Edge weight
1
0.8
0.6
0.4
0.2
0

Fig. 5

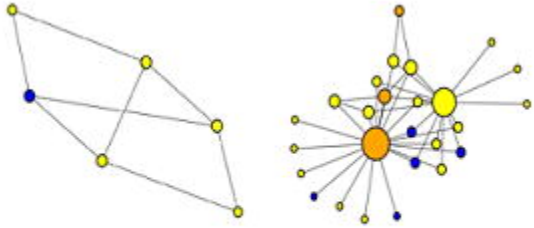

Normal Network State | **Hypersynchronous State (mini-seizures or seizures)**

Synchronizability of network (Fiedler Eigenvalue)	**Low**	**High**
Synchronization strength (average giant connected component edge weight)	**Low**	**High**
Synchronization hubs (Degree variance of nodes)	**Low**	**High**

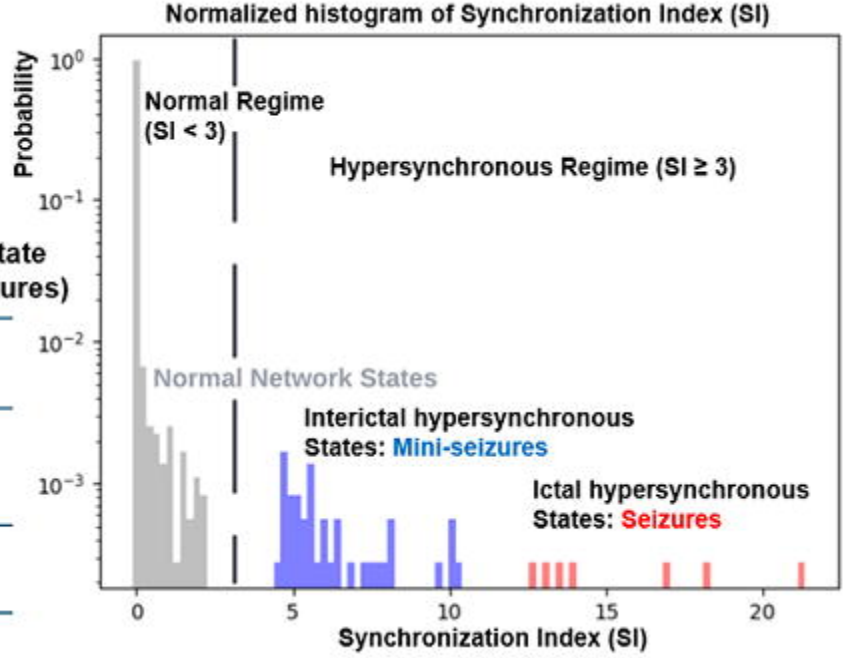

Fig. 6

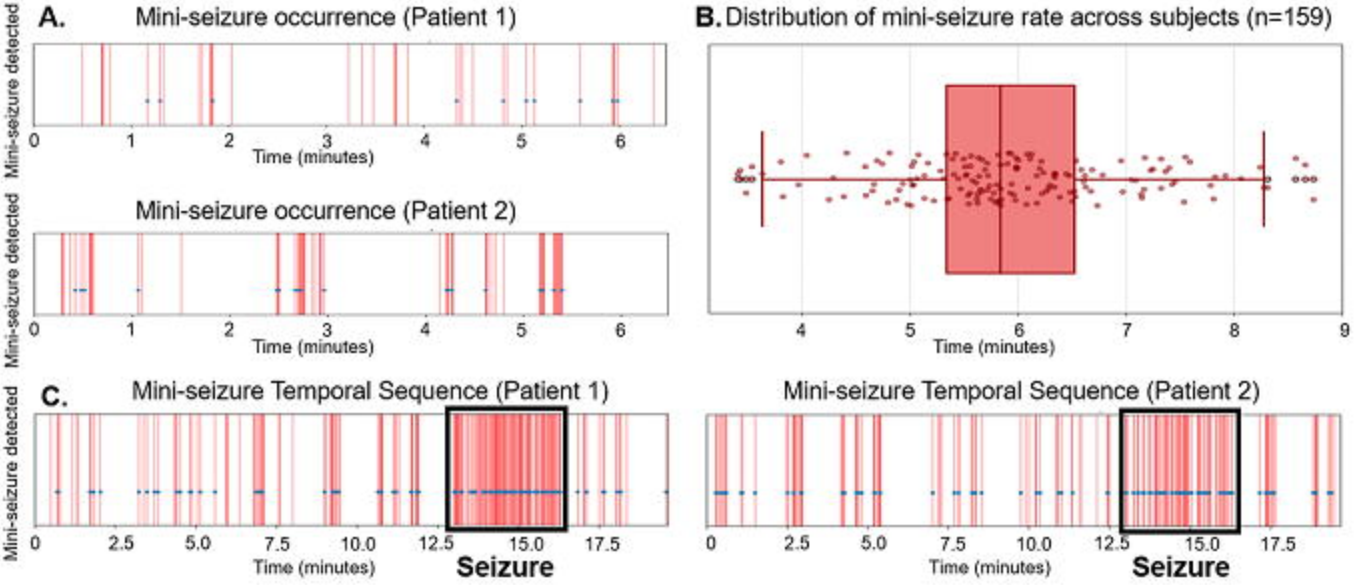
A.
Mini-seizure occurrence (Patient 1)
Mini-seizure detected
0
1
2
3
4
5
6
Time (minutes)
Mini-seizure occurrence (Patient 2)
Mini-seizure detected
0
1
2
3
4
5
6
Time (minutes)
B. Distribution of mini-seizure rate across subjects (n=159)
4
5
6
7
8
9
Time (minutes)
C.
Mini-seizure Temporal Sequence (Patient 1)
Mini-seizure detected
0
2.5
5.0
7.5
10.0
12.5
15.0
17.5
Time (minutes)
Seizure
Mini-seizure Temporal Sequence (Patient 2)
0
2.5
5.0
7.5
10.0
12.5
15.0
17.5
Time (minutes)
Seizure

Fig. 7

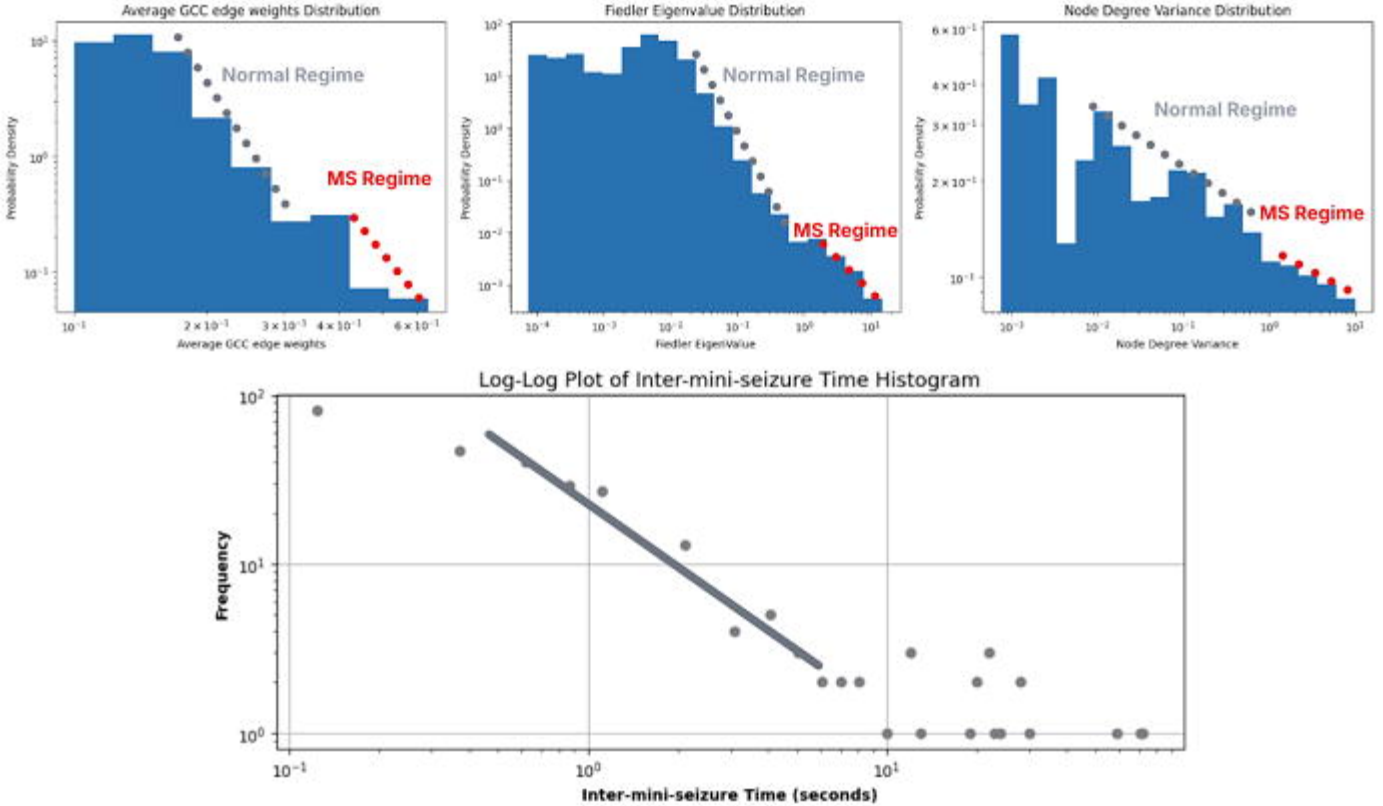
Average GCC edge weights Distribution
Normal Regime
MS Regime
Probability Density
Average GCC edge weights
Fiedler Eigenvalue Distribution
Normal Regime
MS Regime
Probability Density
Fiedler EigenValue
Node Degree Variance Distribution
Normal Regime
MS Regime
Probability Density
Node Degree Variance
Log-Log Plot of Inter-mini-seizure Time Histogram
Frequency
Inter-mini-seizure Time (seconds)

Fig. 8

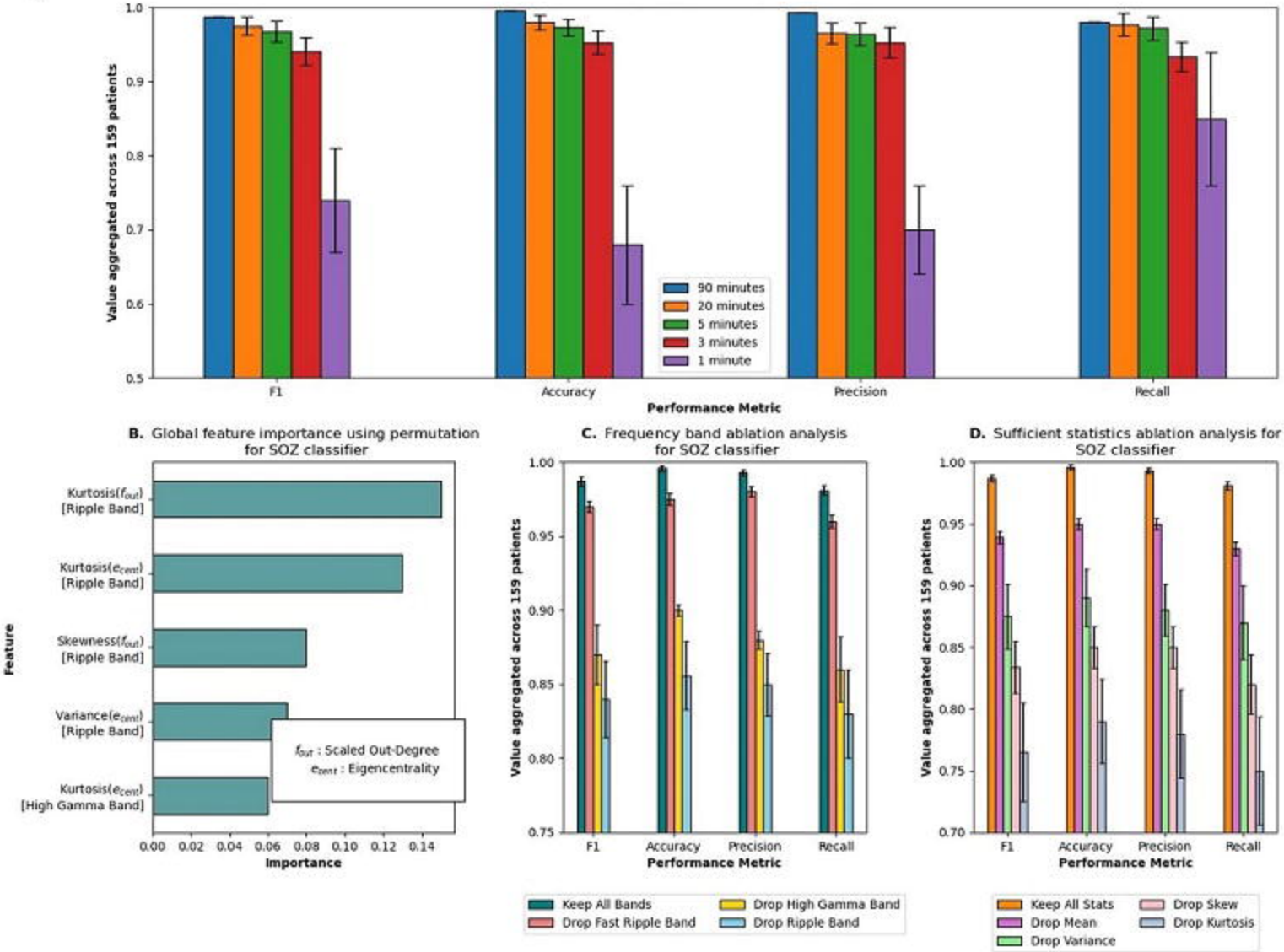

Note: y-axis on bar charts does not start at the origin.

Fig. 9

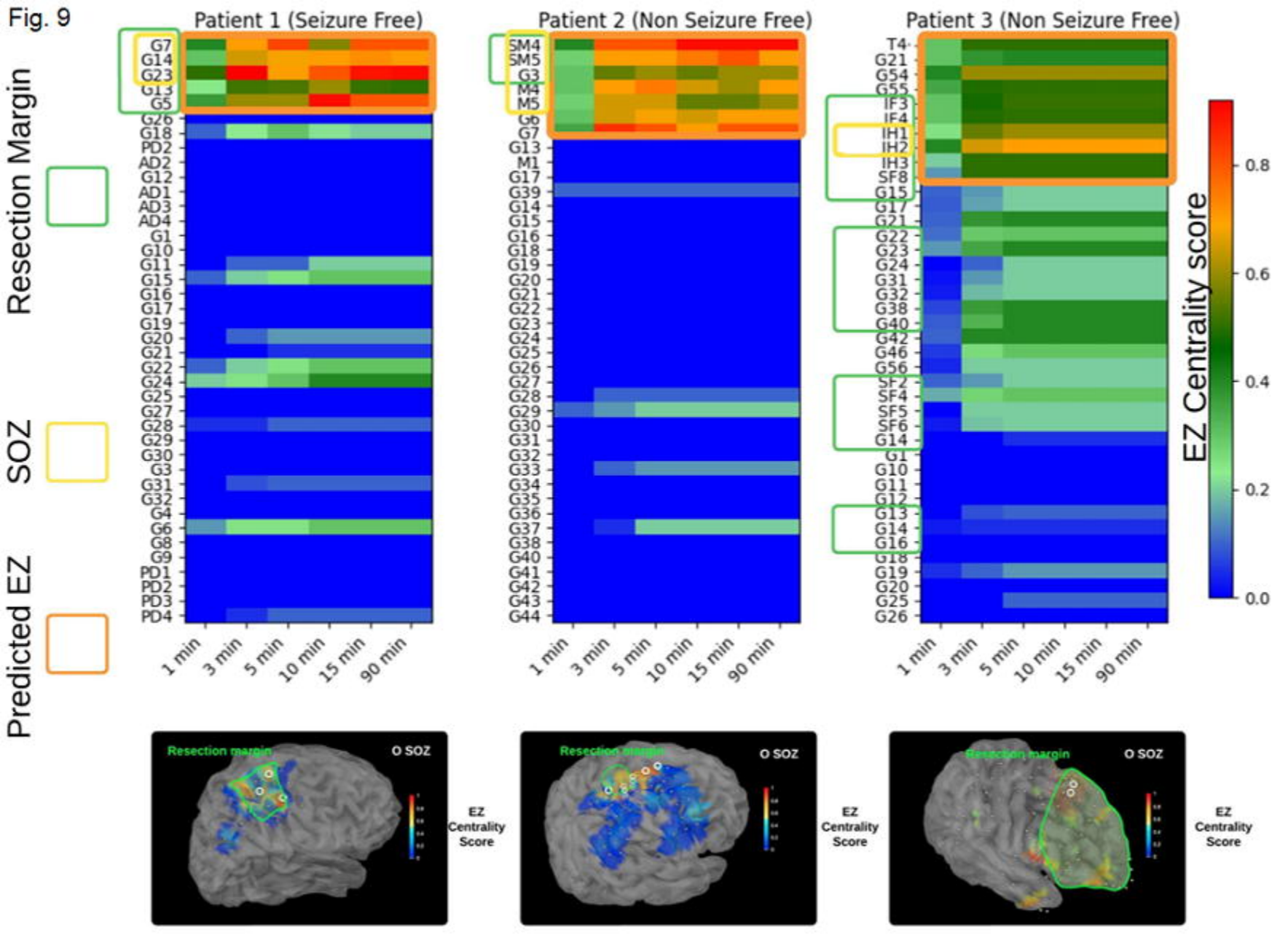
Patient 1 (Seizure Free)
Patient 2 (Non Seizure Free)
Patient 3 (Non Seizure Free)
Resection Margin
SOZ
Predicted EZ
EZ Centrality score
0.0
0.2
0.4
0.6
0.8
1 min
3 min
5 min
10 min
15 min
90 min
Resection margin
O SOZ
EZ Centrality Score

Fig. 10

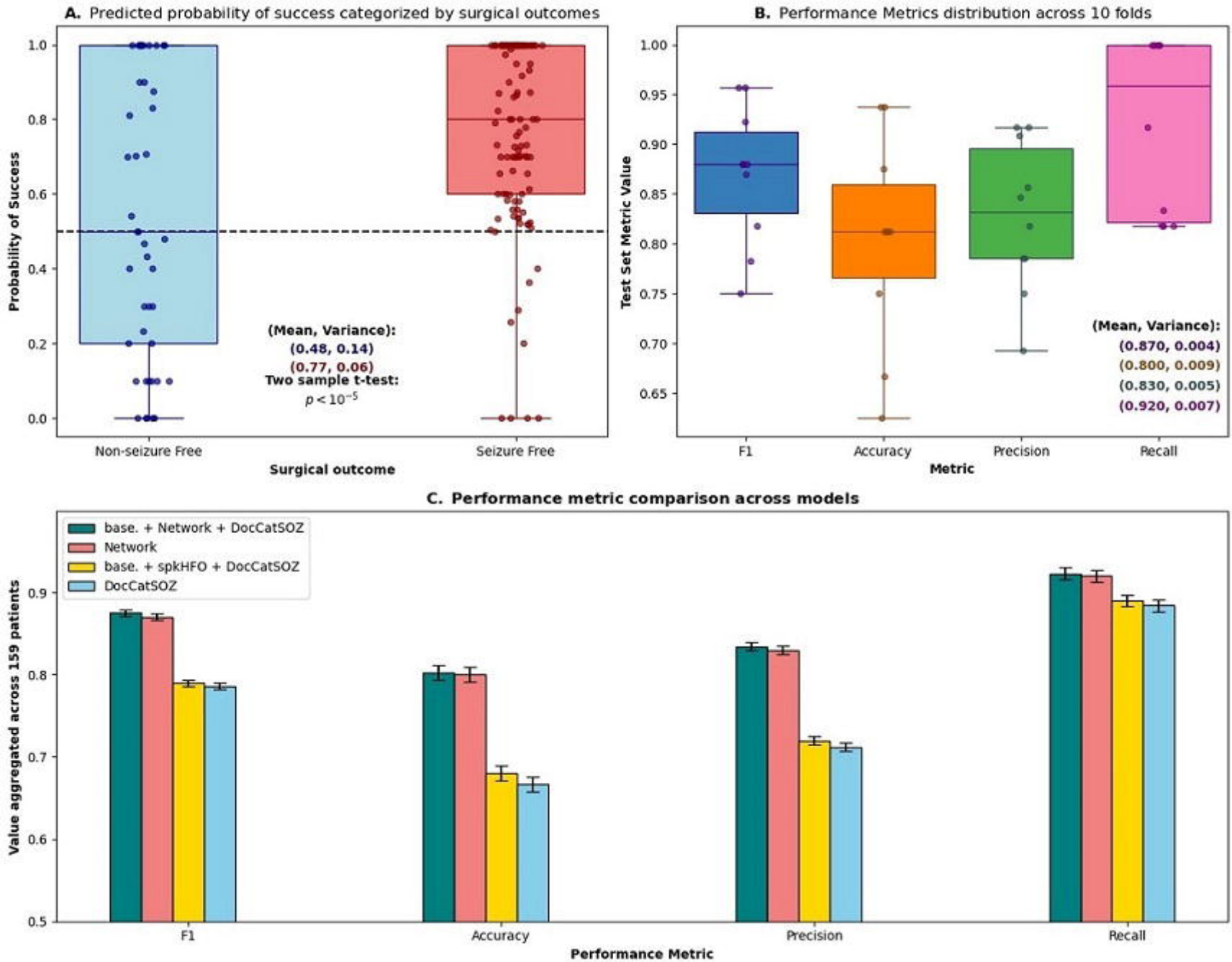
A. Predicted probability of success categorized by surgical outcomes
Probability of Success
1.0
0.8
0.6
0.4
0.2
0.0
(Mean, Variance):
(0.48, 0.14)
(0.77, 0.06)
Two sample t-test:
$p < 10^{-5}$
Non-seizure Free
Seizure Free
Surgical outcome
B. Performance Metrics distribution across 10 folds
Test Set Metric Value
1.00
0.95
0.90
0.85
0.80
0.75
0.70
0.65
(Mean, Variance):
(0.870, 0.004)
(0.800, 0.009)
(0.830, 0.005)
(0.920, 0.007)
F1
Accuracy
Precision
Recall
Metric
C. Performance metric comparison across models
base. + Network + DocCatSOZ
Network
base. + spkHFO + DocCatSOZ
DocCatSOZ
Value aggregated across 159 patients
0.9
0.8
0.7
0.6
0.5
F1
Accuracy
Precision
Recall
Performance Metric

Table 1: Patient Demographics

	UCLA	Detroit	All
Number of patients	24	135	159
Median age in years (range)	13.0 (3–22)	12.0 (4–44)	12.0 (3–44)
Proportion of females (%)	12 (50.0%)	67 (49.6%)	79 (49.7%)
Sampled hemisphere (%)			
Left	12 (50.0%)	61 (45.19%)	73 (45.9%)
Right	9 (37.5%)	51 (37.78%)	60 (37.7%)
Both	3 (12.5%)	23 (17.04%)	26 (16.4%)
Seizure onset zone			
Frontal	13	42	55
Temporal	6	63	69
Parietal	12	49	61
Occipital	3	23	26
Limbic	3	59	62
Patients with postoperative seizure-freedom (%)*	15 (62.5%)	95 (70.4%)	110 (69.2%)
Pathology (%)			
Focal cortical dysplasia	15 (62.5%)	49 (36.3%)	64 (40.3%)
Tumor	3 (12.5%)	28 (20.74%)	31 (19.5%)
Hippocampal sclerosis	0 (0.0%)	11 (8.15%)	11 (6.9%)
Others	6 (25.0%)	47 (34.81%)	53 (33.3%)

*Seizure-freedom is defined as ILAE 1 outcome.